energy&fuels

Article

pubs.acs.org/EF

Atomic Force Spectroscopy Using Colloidal Tips Functionalized with Dried Crude Oil: A Versatile Tool to Investigate Oil−Mineral Interactions

L. Rickard Dickinson,[†] Bart M. J. M. Suijkerbuijk,[‡] Steffen Berg,[‡] Fons H. M. Marcelis,[‡] and Hannes C. Schniepp*[,†]

[†]Department of Applied Science, The College of William & Mary, PO Box 8795, Williamsburg, Virginia 23187, United States

[‡]Shell Global Solutions International B.V., Kessler Park 1, 2288 GS Rijswijk, The Netherlands

Supporting Information

ABSTRACT: The recovery efficiency of water flooding (water injection in oil reservoirs to recover oil) can be improved by modification of the ionic composition of the brine. This effect is attributed to changes in the physicochemical interactions within in the crude oil−brine−rock (COBR) system. To systematically modify these interactions, gain predictive capability, and optimize recovery efficiency, further understanding of these systems is required. Our work introduces a new tool to facilitate the study of interactions in such ternary systems. Utilizing atomic force spectroscopy, we developed a custom dried oil-coated probe which directly measures the interactions between crude oil and a mineral substrate in a varying aqueous environment at their natural length scale. In most of the previous studies, COBR interactions were studied by using model systems wherein crude oil was represented by organic acids, for instance, which is a significant simplification of natural systems that may be unwarranted. In this study, we measured the interaction forces between mineral surfaces and actual crude oils. The experiments allow us to systematically test the effect of brine composition on the forces between mineral surfaces and crude oil components in all their complexity under realistic reservoir conditions. Our results illustrate the reproducibility of measurements made using this custom tool by using multiple probes to show salinity-dependent repulsive interactions between the oil coating and a mica substrate. These electrostatic interactions are consistent with trends expected by the Debye−Hückel theory, showing a decrease in repulsive forces as a function of increasing monovalent ion concentration. Adherence to this expected trend provides insight into the COBR interactions in a particular oil reservoir with particular oil, brine, and mineral compositions. Additionally, the presence of electrostatic forces suggests that the dried crude oil coating retains surface charge throughout the drying procedure. Therefore, this tool has the potential to represent or approximate the electrostatic interactions of the original liquid crude oil system during the study of COBR interactions.

INTRODUCTION

Currently, much of the oil in reservoirs cannot be recovered by conventional methods such as natural depletion, gas injection, and water injection.[1] On average, primary production extracts 10−20% of oil from a reservoir, while water injection increases this extraction to 20−40% of the total oil.[1−3] The recovery is limited by mainly two factors: the macroscopic sweep efficiency, which is impacted by factors like geological heterogeneity, and the microscopic displacement efficiency. Even in cases of optimum sweep, there is a significant amount of oil trapped in the pore space by capillary forces and oil−rock adhesion.[4,5] It has been demonstrated that a promising way to address this problem and increase recovery efficiency is to modify the brine composition of the injection water in order to alter the interactions between rock and crude oil.[6,7]

However, the effectiveness of this approach varies greatly: in some reservoirs the recovered amount of oil improves significantly when the salinity and/or composition of the brine is altered, whereas in other cases the same measures show little to no effect.[8−10] There also appears to be a difference between the ways in which the composition can impact oil recovery from sandstone reservoirs versus carbonate reservoirs. However, the common denominator for both cases is that a change in salinity and pH impacts the surface charge of minerals present in the pore space which is hypothesized by about 80% of the published literature to cause or contribute to the observed low salinity effect.[9,11−18] However, there are also various alternative mechanisms proposed.[10,19−21] Despite significant scrutiny of this subject over the past years, the main reasons for this variation remain rather elusive; our goal is to understand the underlying mechanisms at the pore scale, providing the basis for prediction and systematic optimization of oil recovery.

Systematic analysis of this problem is very complicated because of the compositional complexity of both the crudes and the minerals in the reservoirs, and because of the grain microstructure of the minerals[22,23] and correspondingly heterogeneous oil−water mineral contacts on the pore scale.[18] Reservoir rocks are predominantly composed of silicate and/or carbonate minerals, with great compositional and structural variations depending on the location of the reservoir and the conditions during its formation. The rocks are

Received: July 29, 2016
Revised: October 13, 2016
Published: October 27, 2016

DOI: 10.1021/acs.energyfuels.6b01862
Energy Fuels 2016, 30, 9193−9202

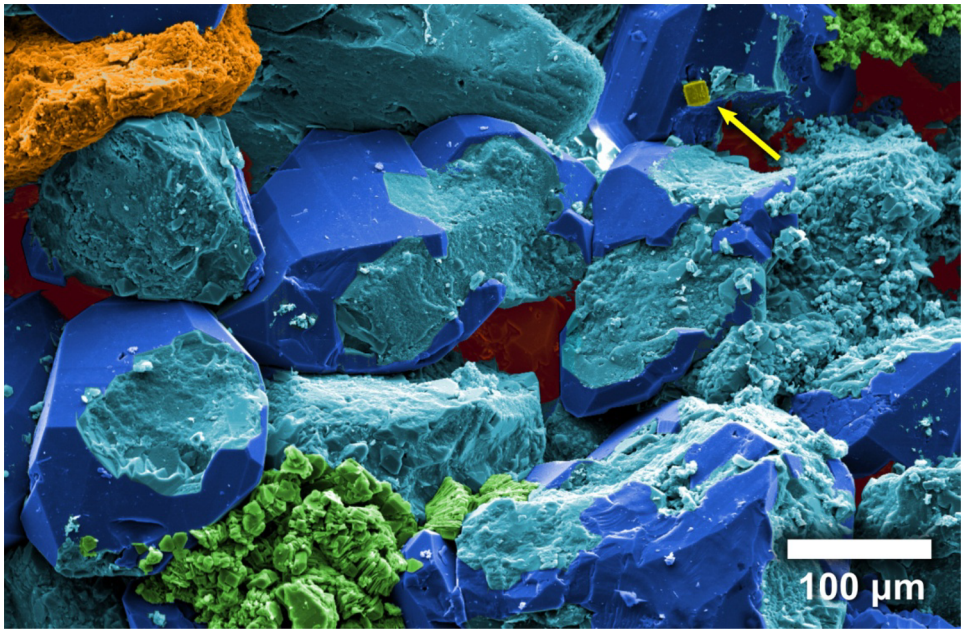

Figure 1. False-color scanning electron microscopy (SEM) image showing the microscopic grain structure of a sandstone sample, featuring secondary quartz (dark blue), fine grained quartz (light blue), a single dolomite crystal (yellow, see arrow), and a detrital claystone grain (orange, top left corner), as well as kaolinite (green) and rock pores (red).

composed of grains from different mineral species, with diameters ranging from micrometers to millimeters and corresponding variations in reservoir porosity (0−25%) and permeability (1−2000 millidarcy).[1] An example is given in Figure 1, which shows a false-color electron micrograph of a piece of Berea sandstone exposing secondary quartz and fine-grained quartz, with the pores between them clearly indicated; patches of kaolinite, a single dolomite crystal, and a detrital claystone grain add further complexity to the sample surface. The surfaces of the different mineral species potentially undergo different chemical reactions in a given brine composition and pH and thus exhibit different surface charge densities. Combined with the rock topography, this can lead to complex, highly heterogeneous surface charge distributions on the rocks. Not only the minerals but also the crude oils exhibit widely different compositions from reservoir to reservoir,[22,24] with varying percentages of naphthenes (hydrocarbons containing cyclic features, 30−60 wt %), paraffins (saturated linear and branched hydrocarbons, 15−60 wt %), aromatics (3−30 wt %),[1] and asphaltenes (heavier hydrocarbons with heteroatoms such as O, N, and S, 0−10 wt %), in addition to small amounts of other chemicals.[1] Crude oil contains a range of components that have polar functional groups and are hence surface active. At the crude oil−brine interface, the functional groups of these components can dissociate and are hence charged.[25] The interactions between the surfaces of the oil droplets and the surfaces of the rocks are determined by factors such as their charges, their chemical compositions, and their topographies. Specifically, the key aspect of both the oil and the rock are their interfaces, not their bulk composition. These interfaces govern the mutual interactions between these components of the subsurface system. Given the complexity of these systems and their compositional variation from location to location, it is not surprising that the relative importance of electrostatic contributions to the oil−rock interactions varies greatly between different reservoirs, and with it the effect of the brines' ionic composition on recovery efficiency.

The most direct way of testing the influence of brine composition on oil recovery efficiency is through spontaneous imbibition tests or core flooding experiments.[26] These experiments are a standard in the oil industry and are typically carried out with crudes and mineral specimens directly from the reservoir and thus take into account the full complexity of these systems;[1] in addition, they also provide the possibility to study the influence of temperature, pH, and salinity on oil recovery.[5,21,27−34] However, these tests cover a wide range of individual aspects, which makes it very difficult to separate individual contributions of different effects and to understand what is cause and what effect. Recent experiments with better control over individual parameters have shown that the adhesion of oil on clay-coated surfaces becomes weaker when lowering the salinity.[11] A disadvantage of all of these methods carried out at a larger scale is that they inherently average over all the mineral components in the reservoir because of the size of the sample that is probed and thus cannot account for specific local geometries. Thus, there is the need to focus more on the details of the oil−solid contacts, which can be consistently and qualitatively described by electrokinetic modeling.[15,35]

Our goal has been to develop predictive capabilities enabling a systematic reduction of oil−mineral adhesion for improved recovery. There is potential for a significantly more rigorous and causal understanding via experiments that avoid averaging over the inhomogeneities of the mineral surfaces and instead focus on the interactions between individual components. This approach further promises the ability to translate interactions from the nano- to microscale to a contribution in an effective surface energy or intrinsic contact angle, in other words, the "scale-up" process from molecular to pore scale.[9] To achieve our goal, there are currently two major directions: contact angle measurements and force spectroscopy (FS) using atomic force microscopy (AFM). For contact angle experiments, a droplet

DOI: 10.1021/acs.energyfuels.6b01862
Energy Fuels 2016, 30, 9193−9202

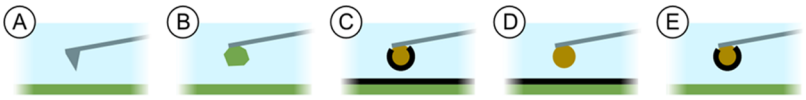

Figure 2. Graphical representation of possible experimental setups to measure oil−mineral interactions via force spectroscopy: using a probe to represent the mineral (A, B, D) or the crude oil (black, C, E), and the substrate as the mineral (A, B, E) or the crude oil (black, C, D). Sharp probes (A) have been used, as well as colloidal probes (B−E).

(typically crude oil or a subset of its components) is placed on top of a smooth substrate of a well-defined mineral species (mica, silicon, silica, kaolinite) to determine wettability as a function of pH,[13,36−40] salinity,[13,36−43] surfactants,[44] solvents,[45] and crude oil composition.[46] One disadvantage of such measurements is that specialized substrates are needed that are pure in composition, smooth enough (to measure an intrinsic contact angle and avoid roughness-induced contact angle hysteresis and other artifacts), and large enough for contact angle experiments. These requirements directly lead to questions regarding the representativeness of such materials for the subsurface. Moreover, such substrates are very challenging to produce for some of the mineral species relevant in reservoir rocks. Another disadvantage is that contact angle measurements essentially probe the interfacial energies[47] without revealing further details about the actual nature of the interactions involved. The latter problem is addressed by FS[48] based on liquid-cell AFM, which has proven very powerful to directly characterize these interfacial interactions. Furthermore, FS is able to directly determine the surface forces computed in the framework of the Debye−Hückel theory[47] on the basis of surface charges obtained by zeta-potential measurements.

In FS, the interaction forces between a nano- or microscopically small probe and a solid surface, immersed in a liquid medium, are directly probed as a function of separation, with subnanometer and piconewton resolutions of separation and force, respectively. The general idea is that the materials used on the surfaces of the AFM probe and the sample are similar enough to the oil and minerals such that the measured forces are representative of the oil−mineral interactions in a reservoir. The liquid cell can be loaded with different brines to simulate waterflooding conditions and test the effects of brine composition.

A particular difficulty in FS is the preparation of the probe and solid substrate such that the conditions in a reservoir are approached and the measurements actually probe the oil−mineral interactions. For the AFM probe, two geometries have been employed: In a minority of the cases, regular "sharp" AFM probes featuring diameters of a few nanometers have been used[49,50] (Figure 2A). More common are spherical (colloidal) probes featuring radii of a few micrometers (Figure 2B−E).[39,40,51−57] Because of their larger size, colloidal probes are mechanically less fragile than sharp AFM probes; in addition, the larger colloidal probes provide stronger signals, and their spherical geometry can be more easily compared to available models. Regular AFM tips, in contrast, are optimized for sharpness but do not feature a well-defined geometry. When it comes to the materials used for the probe and the substrate, a variety of setups have been used. In a few experiments, the same material was used for tip and substrate (Figure 2B,C). This approach can be used to test the effect of brine composition on the interfacial behavior of only one reservoir component. This has been done for mineral components (Figure 2B) such as Illite (where Illite particles were used as both the substrate and as a "pseudo spherical" colloidal probe).[58]

Introducing a surface representing the oil phase into the system is particularly challenging, because it requires functionalization of at least one surface to mimic the crude. In some cases, both the substrate and the colloidal probe were functionalized with substances to represent the oil (see Figure 2C).[40,56,57] The most representative approach, however, to studying oil−mineral interactions with FS is to represent both the oil and the mineral in the system. Therefore, either the probe takes the role of the mineral and the substrate takes the role of the crude (Figure 2D)[39,54,55] or vice versa (Figure 2E).[49,50,52,53] A disadvantage with the former approach is that colloidal spheres are available only in a very limited range of materials; the sphere material closest to any of the mineral components in reservoirs is amorphous silica, which was used in multiple references.[39,54,55] It is chemically similar but not identical to quartz;[22] for other mineral species found in reservoirs no colloidal spheres with similar surface chemistry are available. This problem can be addressed by having the probe represent the oil and the substrate represent the mineral (see Figure 2E). Because the only requirement for the substrate is to be flat, many more materials become viable, and many more of the mineral surfaces found in a reservoir can be probed. For example, researchers have measured the interactions on the following simulated minerals: silicon,[50] Illite,[50] mica,[50−52] glass,[52,53] and sandstone grains.[49]

A final question is with which material we should functionalize the probe to best represent the crude, which is challenging because of the complexity of crude oil. Most of the studies have used a single substance, such as octadecane[51] or *n*-decane,[54] to represent the crude; in other cases, individual functional groups, such as −COOH[49,50] and $-CH_3$,[50] were used to simulate polar or nonpolar oil interactions with minerals. While this dramatically simplified approach provides well-defined experimental conditions, it remains unclear whether this provides a realistic approximation to the behavior of real crude. Some other experiments used a subset of the crude oil components for functionalization, such as bitumen,[40,56] resin,[53] and asphaltenes.[53,57] Our goal was to stay as close as possible to the conditions in the reservoir; therefore, we decided to use actual crude oil for functionalization. Hogshead et al. had previously used crude to functionalize substrates;[55] however, as detailed in the previous paragraph, this means that the probe has to be used to represent the mineral, which has several disadvantages. To overcome this limitation, one can functionalize the AFM probes with crude, which has previously been demonstrated by Basu and Sharma, who determined the critical disjoining pressure between a crude-coated colloidal probe and a water film.[51−53] A problem they found in their work is that the oil pulls off the tip over time, and tips thus need to be changed frequently.[51−53]

In the work presented here, we build on the idea of functionalizing a colloidal AFM probe with crude oil. This approach provides the ability to study the interactions with a

DOI: 10.1021/acs.energyfuels.6b01862
Energy Fuels 2016, 30, 9193−9202

wide range of minerals, which are introduced as solid substrates. However, we sought to develop a crude oil-coated probe that is capable of conducting many measurements without significant oil loss. Such a probe enables longer-term experiments, for example to monitor oil−mineral interactions as a function of changing solution composition without changing the probe. We show that coating a colloidal AFM probe in crude oil and then allowing the lighter components to evaporate provides a robust oil layer that can be used to probe interactions with mineral surfaces in aqueous solutions. This initial study tests electrostatic forces as a function of salinity and shows that our dried oil probe still holds electrostatic charges after the drying process and thus exhibits electromagnetic interactions similar to those of crude oil.

EXPERIMENTAL SECTION

Materials. We used freshly cleaved mica (Ted Pella; PELCO, grade V5) as an atomically smooth and homogeneous substrate. Sodium chloride (Sigma-Aldrich; Certified ACS grade) and picopure water (Synergy UV Millipore) were used to make the solutions. The crude oil that we utilized for coating both the wet and dried oil probes comes from an Asian oil field and was sampled at the well head to prevent contamination with production chemicals. The total acid number (TAN) of this crude was ≈0.25, determined according to ASTM Standard D 664. We built the colloidal probes from nonfunctionalized silica spheres (Bangs Laboratories; mean diameter, 7.27 ± 0.702 μm), tipless silicon nitride cantilevers (Bruker; MLCT-O10; nominal spring constant k = 0.05 N/m), and 5 min quick-set epoxy (Ace Hardware). Cantilevers with a relatively low spring constant were chosen to measure the weak electrostatic interactions.

Manufacturing Crude-Functionalized Colloidal Probes. To make the colloidal silica probes we attached the AFM probe to a three-dimensional translation stage which was mounted to an Olympus iX71 inverted optical microscope. The following microscope objectives were used for all analysis and to make the colloidal probes: MPLFLN-BD, 5× (0.15 NA); MPLFLN-BD, 20× (0.45 NA); and MPLFLN-BD, 100× (0.9 NA). The manufacturing process is illustrated in Figure 3.

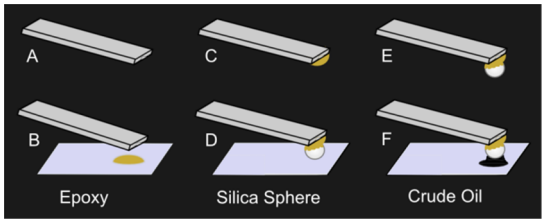

Figure 3. Steps detailing the manufacturing procedure of our custom AFM probe.

To make the probes, a tipless cantilever (Figure 3A) was dipped into an epoxy droplet that had previously been deposited onto a glass slide (Figure 3B) to attach a small amount of epoxy to its end (Figure 3C). The epoxy-coated cantilever was then brought into contact with a silica sphere on the same glass slide in order to glue it to the cantilever (Figure 3D). After the epoxy cured and the silica sphere was firmly attached to the cantilever (Figure 3E), we dipped the probe into a droplet of crude oil (Figure 3F). At this stage of the preparation process, we classify it as a "wet" oil probe because the oil coating on the sphere is still liquid.

For reference purposes, we did some experiments with the "wet" probes described in the previous paragraph; most probes, however, were further treated and converted into "dried" probes. Therefore, they were placed in an oven (Thermo Scientific; Lindberg Blue M V0914A vacuum oven) at 50 °C and ambient pressure to evaporate the more volatile components in the oil and solidify the oil coating. After removal from the oven, the probes remained in ambient conditions until the experiments were performed. This time span varied from a few hours to 5 days. A bare silica probe and the surface of a dried oil-coated probe were imaged via SEM using Amray 1810 and Hitachi S-570 instruments. For SEM sample preparation, a gold/palladium coating was applied using an Anatech Hummer 6.2 sputter coater.

Force Spectroscopy. To study the effect of the salinity, we performed FS experiments (NT-MDT; Ntegra Prima) for each probe in a higher-salinity environment (10 mM NaCl) at multiple locations on a mica substrate, followed by the lower-salinity measurements (1 mM NaCl). The experiments were performed at ambient temperature and pressure. A closed liquid cell (NT-MDT; model MP3LCNTF) was used to prevent changes in the concentration due to evaporation. We then converted the raw FS force−displacement curves to true force−distance curves.[48] As the first step of this process, we vertically shifted all curves such that the zero of the deflection axis corresponds to the relaxed cantilever. This process also removes the vertical offset among curves resulting from the gradual drift of the cantilever during an experiment. Second, we applied a linear fit to the constant compliance region (in which the probe establishes "hard" contact with the surface) and shifted the curves horizontally such that the linear fit went through the origin. This procedure also defines the zero of separation. Finally, we scaled the data (so that the "hard" contact region represents the linear elastic response of the cantilever), converting the piezo extension to a tip−sample separation value and scaling of the data to units of force (based on the spring constant of the cantilever).

pH Measurements. To ensure that our results were not influenced by pH changes, we took five pH readings from the solution in the liquid cell after each experiment (Oakton Instruments; CON 510 Series, using a Thermo Scientific Orion 9110DJWP Double Junction pH Electrode). The measured pH was compared to pH measured in the original stock solutions used to feed the liquid cell (Figure 4). These tests were done because changes in the pH would

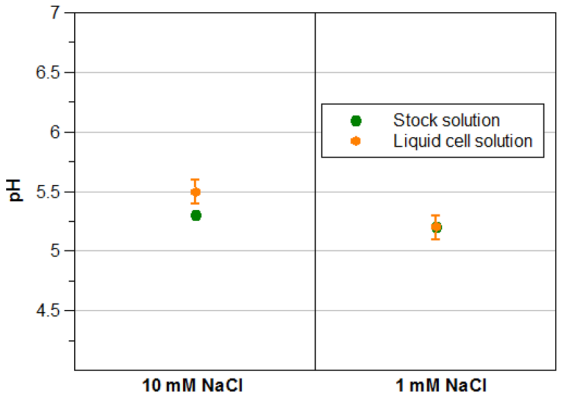

Figure 4. Stock solution (before experiment) and liquid cell solution (after experiment) pH averages for 10 mM NaCl and 1 mM NaCl (standard deviation given in the error bars).

potentially affect the charges of the investigated surfaces and thus their wetting behavior.[47] We found the pH values to be very stable; for the 10 mM NaCl concentration, the measured pH was slightly higher after the experiment (5.5 ± 0.1) compared to before (5.3 ± 0.0). For 1 mM NaCl, there was no measurable pH difference before (5.2 ± 0.0) and after (5.2 ± 0.1) the experiment. For the mica substrate, such little pH changes will not modulate the surface charge substantially, because the isoelectric point of mica is much lower (pH 3−3.5).[59] The oil surface may, however, be more susceptible to changes as the pH values are around the pK_a of carboxylic acids, which occur in crude oils. The isoelectric point of the crude oils we used is not known. The overall relatively low pH values are due to ingress of ambient CO_2 into the stock solutions. The measured pH values around 5.5 are still, however, relevant to actual reservoir conditions.

DOI: 10.1021/acs.energyfuels.6b01862
Energy Fuels 2016, 30, 9193−9202

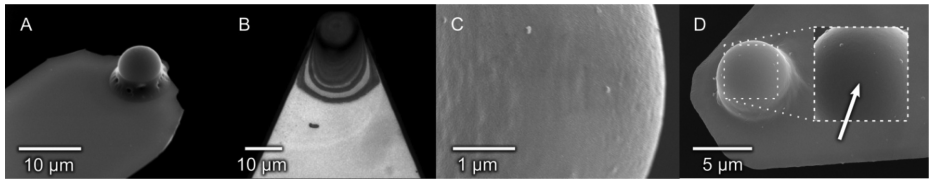

Figure 5. (A) SEM image of an uncoated, homemade FS probe, featuring a 7 μm diameter silica sphere glued to the end of a tipless AFM cantilever using epoxy. (B) Similar probe after coating it in crude oil and drying (using a different cantilever model). Interference fringes are apparent in the dried crude oil. (C) SEM image of the surface of the dried oil on the silica sphere. (D) SEM image of a dried-oil probe after completing a full set of force spectroscopy experiments. Inset: larger magnification, approximate contact point of probe with surface indicated by white arrow.

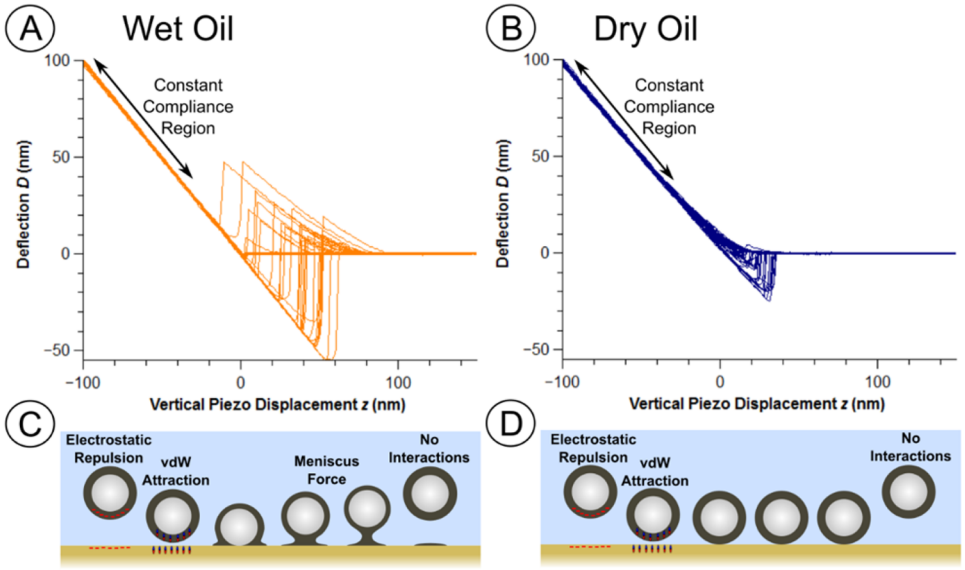

Figure 6. Series of force−displacement curves from both a wet oil-coated probe (A, orange lines) and dried oil-coated probe (B, blue lines). The wet oil probe data (A) shows the electrostatic repulsion and "snap-in" due to van der Waals attraction far from the surface. (C, D) Corresponding schematics of force spectroscopy measurements between an oil-coated probe and a flat, charged substrate as the probe approaches, contacts, and retracts from the substrate (left to right). (C) The wet oil-coated probe pushes through its oil layer during contact, before ultimately making hard contact between the silica sphere and the substrate. (D) The thin, dried oil layer, in contrast, directly provides a hard surface itself.

RESULTS AND DISCUSSION

Characterization of Crude-Functionalized Probes. The SEM image in Figure 5A shows one of our homemade colloidal probes before coating it in crude oil. The image shows that the epoxy attaches the sphere to the lever but does not contaminate the silica sphere. As a nondestructive method to inspect and monitor the crude-coated and dried probe we used an inverted optical microscope. We typically saw optical interference patterns in the optical images, introduced by the oil coating on the probe (see Figure 5B); such patterns can be used to estimate the thickness of the coating. Optical micrographs of the same probe at different stages of the drying process revealed a change in the interference pattern consistent with a thinning of the coating, which is due to the loss of the volatile components during the drying process. We considered the crude oil coating to be "dried" when the interference patterns on the cantilever surrounding the probe no longer changed with additional time spent in the oven. Depending on the thickness of the oil layer, this state was reached after different durations in the oven, ranging from 30 to 47 h. As the SEM image in Figure 5C shows, the oil forms a uniform coating over the surface of the sphere without any cracks or other deformations in the coating. We also completed a set of SEM images of several probes after completing the force spectroscopy experiments; a typical image is shown in Figure 5D, including an inset featuring higher magnification. We did not find any evidence for loss of oil, flattening of the oil layer on the surface, nor any other sign of damage or wear at the apex of the probe where contact with the substrate is expected (position highlighted by white arrow).

Force Curves of Wet versus Dried Oil Probes. Using our wet oil-coated and dried oil-coated probes we carried out force spectroscopy measurements on mica substrates. Mica was chosen for two reasons. On one hand, it provides a clean, atomically flat substrate, avoiding topography-induced force variations. On the other hand, as a silicate mineral it is chemically similar to the clay platelets omnipresent on the surfaces of reservoir rock, specifically Illite.[60] Because mica is a natural mineral and thus potentially inhomogeneous, we collected force curves on multiple locations for averaging purposes.

Figure 6 shows raw data from both wet oil (A) and dried oil (B) probe experiments. To compare the results from the two different experiments, the arbitrary offsets inherent to raw force curves were eliminated as follows: deflection (dependent variable, on the vertical axis) is plotted relative to the relaxed state of the cantilever observed at large separations; cantilever displacement (independent variable, on the horizontal axis) is plotted relative to the hypothetical extrapolated hard contact point between the undeflected probe and the sample. This

DOI: 10.1021/acs.energyfuels.6b01862
Energy Fuels 2016, 30, 9193−9202

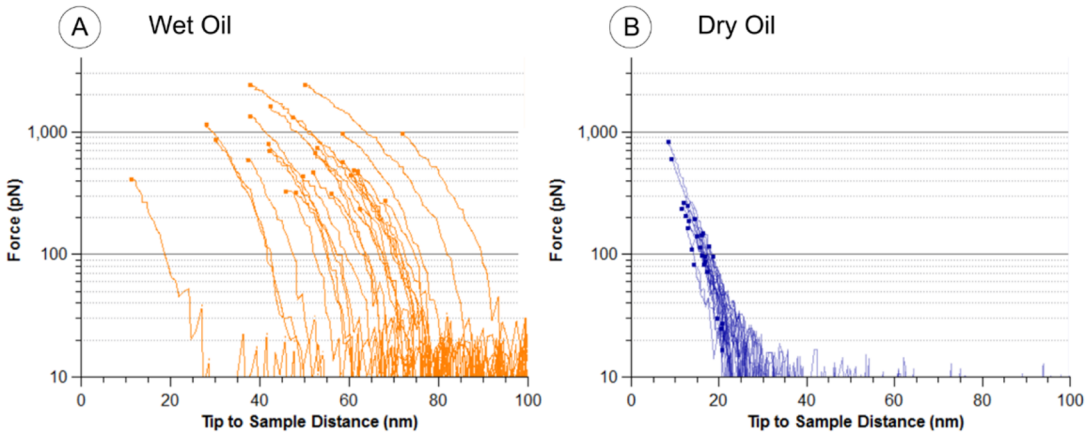

Figure 7. Repulsive region of processed curves from Figure 6 plotted with a logarithmic force scale to indicate deviation from an exponential trend. The maximum force in each curve is indicated by a scatter point.

process is described in Experimental Section as the first two steps in the curve processing procedure. Accordingly, all curves exhibit zero deflection, D, at large displacements; they then feature a gradual onset of repulsive forces (upward cantilever deflections D) as the probe approaches the surface (decreasing displacements z) for both the wet and the dried oil probe. However, the onset of repulsion of the wet oil in Figure 6A occurs at much greater piezo displacements z and features a large scatter in these displacements compared to the dried oil (Figure 6B), which can be explained as follows. For the wet oil probes consisting of a silica sphere covered in a wet oil layer (see Figure 6C), it is actually the silica sphere below the liquid oil layer that establishes hard contact with the substrate and thus defines the constant compliance region (indicated in Figure 6A), whereas the repulsive electrostatic interaction occurs between the outer surface of the liquid oil covering the silica sphere. Hence, there is an offset between the electrostatic interactions and the hard repulsion, corresponding to the thickness of the oil layer. This thickness varies from probe to probe and can also decrease during the experiment, in cases where the amount of oil on the probe is reduced because of transfer to the substrate. Moreover, because of its mechanical instability, the oil–water interface is also subject to random motions, thus introducing noise. The corresponding variations in this offset can be observed in Figure 6A. Because the layer thickness is unknown, and because tip separation in AFM is determined only relative to the hard contact point, we have found it impossible to quantitatively determine the actual separation of the liquid oil surface from the substrate. For the dried oil probe, in contrast, it is the surface of the dried oil, and not the silica sphere below it, that establishes contact with the substrate (Figure 6D) in the constant compliance region. Correspondingly, there is no offset in Figure 6B. This demonstrates that the dried oil probes have several advantages: the interaction distance between the oil surface and the substrate can be quantitatively determined; the results are much more reproducible, and they do not directly depend on the thickness of the applied oil layer.

Quantitative analysis of force spectroscopy data is challenging when the surface of the probe can deform significantly as a function of separation,[61,62] which is the case for the wet oil. The apparent oil–mica repulsion increasingly pushes the oil surface away from the mica as the probe comes closer to the surface. This systematic deformation of the interface leads to a deviation from the expected[47,63] exponential behavior and thus complicates comparison of the experimental data to models. To test our experimental data for the presence of this phenomenon, the curves from Figure 6 were converted to force–distance curves and plotted in Figure 7 with a logarithmic force scale. It is apparent that the curves from the wet oil probes are not straight lines (Figure 7A), as would be expected for exponential functions, but systematically deviate toward smaller forces at shorter distances. This can be explained by the compression of the oil layer due to repulsive forces, which gradually increases the actual separation between the surfaces during approach and thus lowers the repulsive forces. For the dried oil probe, in contrast, the force curves show the expected exponential trend over the entire distance (Figure 7B). The suspected flattening of the wet oil droplet would also be expected to increase the effective probe–substrate interaction area. This is consistent with our observation that the maximal repulsive force, indicated by scatter points at the end of each plotted curve in Figure 7, was systematically higher for the wet probes (0.8 ± 0.6 nN) in comparison to the dried probes (0.1 ± 0.2 nN).

The fact that the separation measurements for the wet oil probe are dependent on the varying thickness of the oil layer particularly complicates the fitting procedure. Usually, this region of the true force–distance curve, $F(d)$, is fitted with a function of the form

$$F(d) = A \cdot e^{-d/\lambda} \quad (1)$$

where λ is the Debye length[47] and A is the electrostatic repulsion at zero separation. However, an additional offset, Δd, due to the liquid layer on the probe will introduce a potentially very large artificial correction $e^{\Delta d/\lambda}$ to the fit parameter A, with no direct meaning in terms of an actual electrostatic force. Correspondingly, in case of a wet oil coating on the probe, A is no longer a quantitative measure for the absolute strength of the electrostatic repulsion. This made it impossible for us to quantitatively compare the strength of the electrostatic repulsion measured with liquid coatings of different thickness. Our newly developed dried oil probes avoid all of these difficulties and thus allow for a more quantitative analysis of the force data.

Application of Dried Oil Probes. To demonstrate the versatility and durability of our dried oil probes, we carried out a series of FS experiments on mica, using three different probes ("1", "2", and "3"), all coated with the same type of crude oil.

DOI: 10.1021/acs.energyfuels.6b01862
Energy Fuels 2016, 30, 9193–9202

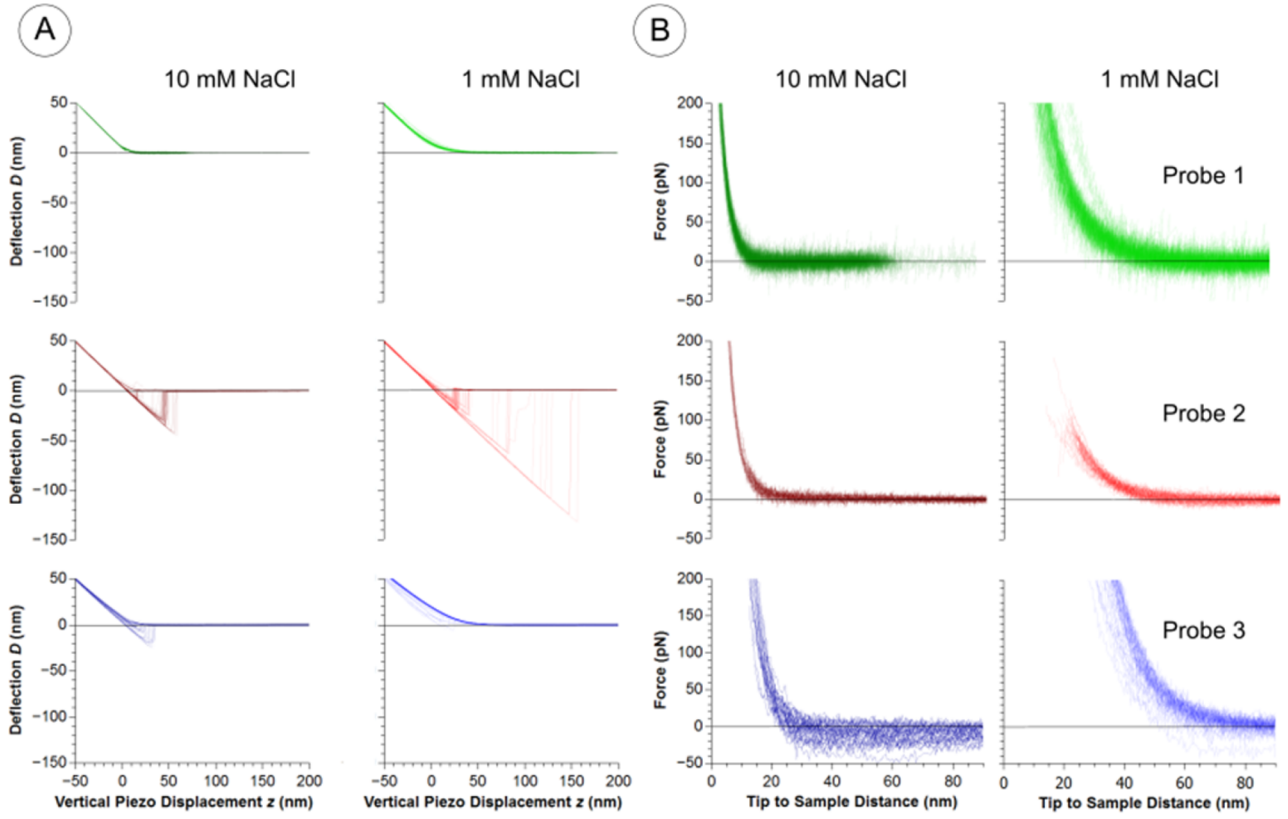

Figure 8. Force–displacement curves for dried oil probe (A) and corresponding true force–distance curves that exhibited repulsion (B).

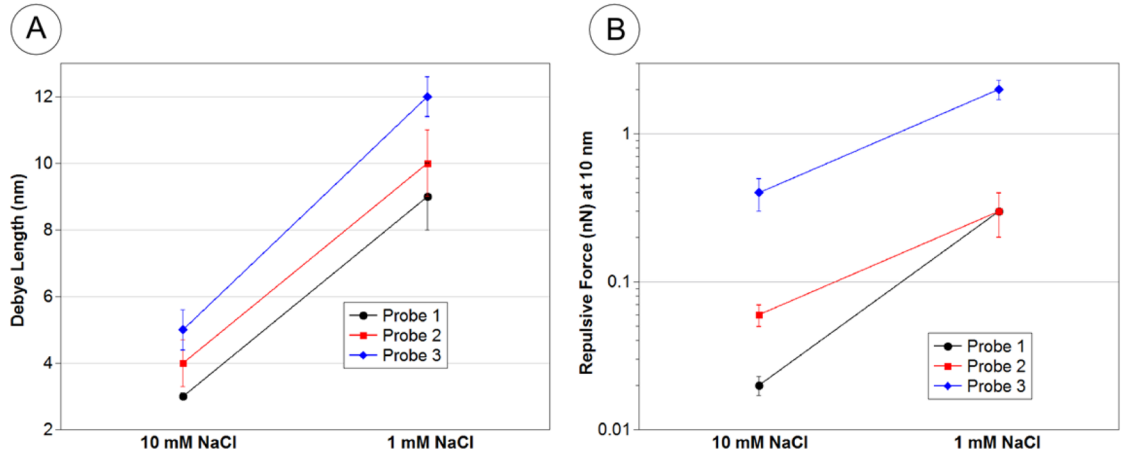

Figure 9. Average Debye length of exponential fits taken from processed repulsion curve data (A) and average electrostatic repulsion values at 10 nm separation distance between the three custom probes and mica substrate at two different liquid cell solution molarities (for a total of six scatter points) (B). For these solution molarities, the calculated Debye lengths based on theory are 3.0 nm (10 mM NaCl) and 9.6 nm (1 mM NaCl).[47]

Each force spectroscopy experiment was carried out in 10 mM and 1 mM aqueous NaCl solutions in order to study electrostatic interactions as a function of salinity. Figure 8 summarizes all of our data taken from the three different probes at the two salinities, showing both the approaching force–displacement curves (A) and corresponding true force–distance curves (B). In Figure 8A (force–displacement curves) 98% of all individual force curves collected are shown; only about 2% of the curves had erratic shapes, for instance when the probe never disengaged from the surface. Some curves for probes 2 and 3 exhibited van der Waals attraction (Figure 8A), while the curves for probe 1 did not.

In Figure 8B only the curves from Figure 8A that exhibited measurable repulsion (75% of all curves) are plotted as true force–distance curves. The remaining curves either exhibited no repulsion (20%) or exhibited repulsion far from the surface (3%; predominantly isolated to probe 2). Relying on the 75% of curves that exhibited measurable electrostatic repulsion (Figure 8B), we sought to quantitatively compare the effect of salinity on electrostatic forces between the oil coating and mica substrate. Therefore, we computed the Debye length for each individual true force–displacement curve by carrying out an exponential fit; averages and standard deviations (error bars) are shown in Figure 9A. Based on Debye–Hückel theory,

DOI: 10.1021/acs.energyfuels.6b01862
Energy Fuels 2016, 30, 9193–9202

Debye lengths were calculated to be 3.0 nm (10 mM NaCl) and 9.6 nm (1 mM NaCl).[47] For all three of our probes, the Debye length increases as the salinity decreases, as expected. For probes 1 and 2, the measured Debye lengths are within expectations of the theory; probe 3 showed Debye lengths slightly higher than expected.

We were further looking for a useful metric in order to quantify the strength of the electrostatic repulsion. In principle, one could use the A value of the exponential fits (eq 1), which has the interpretation of representing the strength of the electrostatic force at zero distance. However, we do not consider this to be the best way to characterize electrostatic interactions, because van der Waals forces are very significant, potentially dominant, at such short separations. Moreover, it turned out that the A value is not very robust with respect to fitting errors in λ, especially because the measured force curves usually do not extend all the way to $d = 0$ because of snap-in events (see the Supporting Information for an example of a curve exhibiting both electrostatic repulsion and a snap-in event). The metric we used instead to describe the strength of the electrostatic repulsion was to use the fitted functions and take the magnitude of the force at a distance of $d = 10$ nm. At this separation the force curves usually contain data; thus, the fits are a good representation of the measured data (see the Supporting Information for a more detailed discussion of this choice of metric). Also, van der Waals forces are insignificant at this separation; hence, the strength of the electrostatic repulsion at this distance may be a good indicator of the stabilization of a charged mineral surface against adsorption of a charged oil droplet. The values obtained from fits for all three probes at the two different salinities are shown in Figure 9B. Each scatter point represents the average force at $d = 10$ nm for all the processed repulsion curves in Figure 8B (force values from 30−63 curves per scatter point, depending on the probe and solution salinity).

As our data shows, we found significantly increased electrostatic forces at the lower salinity for each of the three probes. This is in agreement with the DLVO theory: more ions increase the screening and thus reduce electrostatic forces.[47,64,65] The similar and consistent electrostatic repulsion trends demonstrated by these three different custom probes show the reproducibility that can be achieved with the dried oil probe. The probes were robust enough to carry out a relatively large measurement series. This led to experimental data of better quality compared to the data obtained with wet oil probes. This enables more challenging experiments, like measurements directly comparing different minerals with one AFM probe.

One remaining challenge with our probe is that the absolute amount of force measured varies from probe to probe, with probe 3 exhibiting a greater magnitude of repulsive forces than the other probes. We attribute this variability to a possible difference in geometry of the probe, because the dried oil layer may deform temporarily when contacting the mica substrate. The surface curvature would flatten accordingly, resulting in a larger effective probe−sample interaction area. Such variations in deformation may also stem from the different thickness and stiffness of the oil layer on each probe. As a matter of fact, optical images of the probes suggest that probe 3 was dipped more deeply into the oil droplet than the other two probes when it was made and therefore probably has a thicker layer of oil, which would be expected to be susceptible with respect to temporary surface deformation. Similarly, we found that probe 2 had a thicker oil layer than probe 1, which also correlates with a higher Debye length. These findings indeed suggest that the thickness of the oil layer had an effect on the apparent electrostatic behavior of the probes. These differences in oil layer thickness were not intentional; further work may be needed in order to develop better control over the probe manufacturing process and to improve its reproducibility.

Pertinence of Dried Oil AFM Probes. In addition to discussing the advantages of the dried probe, it is important to also consider possible limitations. Our original goal was to design an experiment that mimics the situation in the reservoir as closely as possible. In particular, keeping as much of the compositional complexity of both the crude oil and the minerals, avoiding any modifications of the original components. The main question in this context is to what extent the drying process of the wet oil on the colloidal AFM probes changes the properties of the crude. The drying process of the oil is expected to leave the relatively less volatile, more polar and charged components on the probe as the nonpolar components evaporate.[66] While we are aware of the fact that this process modifies the composition of the crude, we argue that the effect on the interfacial properties is comparatively small. Our principal rationale is that the interfacial properties of the crude are mainly determined by interfacially active compounds, which are charged and/or feature a greater polarizability and thus a higher surface energy. For example, polar molecules such as asphaltenes should remain on the probe providing a charged surface to interact with the mica substrate.[24,67,68] We were particularly interested in the electrostatic behavior of crude oil surfaces and their electrostatic interactions with minerals, and we do not expect the charge-carrying compounds to evaporate during the drying process. The influence of the drying process on the electrostatic behavior of the crude is thus expected to be limited.

Our rationale regarding the electrostatic behavior of dried oil is supported by our experimental data. All of our measurements with wet and dried oil probes indicate repulsive electrostatic forces between the crude-functionalized probes and the mica substrate. Because mica is negatively charged at the pH we used, this means that both the wet and dried oil surfaces also feature a negative surface charge. For wet crude oil surfaces, previous reports indicate that the isoelectric point is typically between 3 and 7.[25,36,69,70] Our results further show that for this particular crude oil both wet and dried oil surfaces indeed have the same (negative) surface charge. However, quantitative comparison of the charge densities on wet and dried oil probes is challenging, because such comparison is hindered by the discussed experimental complications associated with the liquid oil interface.

CONCLUSION

We have demonstrated the advantages of our newly developed "dried oil" AFM probe in FS applications. Other studies have explored the interactions in the crude−water−rock system utilizing FS. However, in contrast to previous studies, our method is based on using actual crude oil rather than relying on individual oil components. Our approach relies on first coating and then drying crude oil onto a colloidal AFM probe. In terms of electrostatic interactions, this dried oil probe behaves similarly to a colloidal AFM probe covered in liquid oil, which suggests that the drying process does not significantly affect the surface chemistry of the probe and that force curves obtained with a dried oil probe can be considered as

DOI: 10.1021/acs.energyfuels.6b01862
Energy Fuels 2016, 30, 9193−9202

representative of crude oil. In comparison to wet oil probes, however, it provides much greater stability and durability, and it provides experimental data of significantly higher quality, as demonstrated by our results. The probe surface is more robust and maintains its geometry; moreover, the obtained force curves establish a point of zero separation, which enables the measurement of absolute probe−sample separations. Because of this robustness, the probes are not deformed as they approach the surface; thus, undistorted force curves can be obtained. The probes are stable enough to allow the completion of many experiments; therefore, quantitative comparisons for interactions with different minerals or in solutions of different composition can be established with the same probe. As is the case in general with scanning probe techniques, such comparative experiments with the same probe are particularly important, because fluctuations in the behavior of different probes are notorious, mainly because of geometrical differences.

In conclusion, the dried oil probe we developed represents a highly versatile tool for quantitative measurement of the interaction forces in a crude oil−brine−rock system. This approach is expected to work with every crude oil in principle, and the size of the probe is small enough to test interactions with individual grains of reservoir rock. We thus believe that this will become a powerful tool to improve our fundamental understanding of crude−mineral interactions.

■ ASSOCIATED CONTENT

Supporting Information

The Supporting Information is available free of charge on the ACS Publications website at DOI: 10.1021/acs.energyfuels.6b01862.

Discussion of a sample force curve and of our metric to assess the strength of the electrostatic interactions (PDF)

■ AUTHOR INFORMATION

Corresponding Author

*Tel.: (757) 221-2559. Fax: (757) 221-2050. E-mail: schniepp@wm.edu.

Notes

The authors declare no competing financial interest.

■ ACKNOWLEDGMENTS

This work was financially supported by Shell Global Solutions International B.V. H.C.S. acknowledges support from the U.S. National Science Foundation under Grant 1534428. We acknowledge William W. Dickinson for help with scanning electron microscopy.

■ REFERENCES

(1) Hyne, N. J. *Nontechnical Guide to Petroleum Geology, Exploration, Drilling, and Production*, 2nd ed.; Penn Well Corporation: Tulsa, OK, 2001.

(2) Lake, L. *Enhanced Oil Recovery*; Prentice Hall: Englewood Cliffs, NJ, 1989.

(3) Lake, L. W.; Johns, R.; Rossen, B.; Pope, G. *Fundamentals of Enhanced Oil Recovery*; Society of Petroleum Engineers: Richardson, TX, 2014.

(4) Agbalaka, C.; Dandekar, A. Y.; Patil, S. L.; Khataniar, S.; Hemsath, J. R. In *SPE Asia Pacific Oil & Gas Conference and Exhibition*; Society of Petroleum Engineers (SPE): Perth, Australia, 2008.

(5) Sharma, M. M.; Filoco, P. R. *SPE Journal* **2000**, *5* (3), 293−300.

(6) Dake, L. *Fundamentals of Reservoir Engineering*, 1st ed.; Elsevier: Oxford, UK, 1978.

(7) Huang, J. S.; Varadaraj, R. *Curr. Opin. Colloid Interface Sci.* **1996**, *1*, 535−539.

(8) Skrettingland, K.; Holt, T.; Tweheyo, M. T.; Skjevrak, I. *SPE Reservoir Evaluation & Engineering* **2011**, *14* (2), 182−192.

(9) Suijkerbuijk, B. M. J. M.; Kuipers, H. P. C. E.; Kruijsdijk, C. P. J. W. van; Berg, S.; Winden, J. F. van; Ligthelm, D. J.; Mahani, H.; Almada, M. P.; Pol, E.; Van den Niasar, V. J.; Romanuka, J.; Vermolen, E. C. M.; Al-Qarshubi, I. S. M. In *International Petroleum Technology Conference*; Beijing, China, 2013.

(10) Zhang, Y.; Morrow, N. R. In *SPE/DOE Symposium on Improved Oil Recovery*; Society of Petroleum Engineers (SPE): Tulsa, OK, 2006; pp 1−14.

(11) Berg, S.; Cense, A. W.; Jansen, E.; Bakker, K. *Petrophysics* **2010**, *51* (05).

(12) Cense, A.; Berg, S.; Jansen, E.; Bakker, K. In *SPE Enhanced Oil Recovery Conference*; Society of Petroleum Engineers: Kuala Lumpur, Malaysia, 2011.

(13) Mahani, H.; Berg, S.; Ilic, D.; Bartels, W.-B.; Joekar-Niasar, V. In *SPE Enhanced Oil Recovery Conference*; Society of Petroleum Engineers: Kuala Lumpur, Malaysia, 2013; pp 1−14.

(14) Mahani, H.; Keya, A. L.; Berg, S.; Bartels, W.-B.; Nasralla, R.; Rossen, W. In *EUROPEC 2015*; Society of Petroleum Engineers (SPE): Madrid, Spain, 2015; pp 1−27.

(15) Mahani, H.; Berg, S.; Ilic, D.; Bartels, W.-B.; Joekar-Niasar, V. *SPE Journal* **2015**, *20* (01), 8−20.

(16) Mahani, H.; Keya, A. L.; Berg, S.; Bartels, W.-B.; Nasralla, R.; Rossen, W. R. *Energy Fuels* **2015**, *29* (3), 1352−1367.

(17) Mahani, H.; Keya, A. L.; Berg, S.; Nasralla, R. In *SPE Reservoir Characterisation and Simulation Conference and Exhibition*; Society of Petroleum Engineers (SPE): Abu Dhabi, 2015.

(18) Schmatz, J.; Urai, J. L.; Berg, S.; Ott, H. *Geophys. Res. Lett.* **2015**, *42* (7), 2189−2195.

(19) Chávez-Miyauchi, T. E.; Firoozabadi, A.; Fuller, G. G. *Langmuir* **2016**, *32* (9), 2192−2198.

(20) Fredriksen, S. B.; Rognmo, A. U.; Fernø, M. A. In *SPE Bergen One Day Seminar*; Society of Petroleum Engineers (SPE), 2016.

(21) Tang, G.-Q.; Morrow, N. R. *J. Pet. Sci. Eng.* **1999**, *24* (2−4), 99−111.

(22) Cuiec, L. E. In *Fall Meeting of the Society of Petroleum Engineers of AIME*; Society of Petroleum Engineers (SPE): Dallas, TX, 1975.

(23) Zhu, Y.; Weng, H.; Chen, Z.; Chen, Q. *J. Pet. Sci. Eng.* **2003**, *38*, 1−11.

(24) Tissot, B. P.; Welte, D. H. *Petroleum Formation and Occurrence*, 2nd ed.; Springer-Verlag: Berlin, 1984.

(25) Buckley, J. S. In *Proceedings of the 3rd International Symposium on Evaluation of Reservoir Wettability and Its Effect on Oil Recovery*; Laramie, WY, 1994; pp 33−38.

(26) Anderson, W. G. *JPT, J. Pet. Technol.* **1986**, *38* (11), 1246−1262.

(27) Aksulu, H.; Håmsø, D.; Strand, S.; Puntervold, T.; Austad, T. *Energy Fuels* **2012**, *26*, 3497−3503.

(28) Austad, T.; Shariatpanahi, S. F.; Strand, S.; Black, C. J. J.; Webb, K. J. *Energy Fuels* **2012**, *26*, 569−575.

(29) Buckley, J. S. *Curr. Opin. Colloid Interface Sci.* **2001**, *6*, 191−196.

(30) Hadia, N. J.; Hansen, T.; Tweheyo, M. T.; Torsæter, O. *Energy Fuels* **2012**, *26*, 4328−4335.

(31) Kumar, M.; Fogden, A.; Morrow, N. R.; Buckley, J. S. *Petrophysics* **2011**, *52* (6), 428−436.

(32) Lager, A.; Webb, K. J.; Black, C. J. J.; Singleton, M.; Sorbie, K. S. In *International Symposium of the Society of Core Analysts*; Society of Core Analysts: Trondheim, Norway, 2006.

(33) Yildiz, H. O.; Morrow, N. R. *J. Pet. Sci. Eng.* **1996**, *14*, 159−168.

(34) Zhou, X.; Morrow, N. R.; Ma, S. *SPE Journal* **2000**, *5* (2), 199−207.

(35) Joekar-Niasar, V.; Mahani, H. *Ind. Eng. Chem. Res.* **2016**, *55* (21), 6227−6235.

(36) Drummond, C.; Israelachvili, J. *J. Pet. Sci. Eng.* **2004**, *45*, 61−81.

DOI: 10.1021/acs.energyfuels.6b01862
Energy Fuels 2016, 30, 9193−9202

(37) Lebedeva, E. V.; Fogden, A. *Environ. Sci. Technol.* **2010**, *44*, 9470−9475.
(38) Lebedeva, E. V.; Fogden, A. *Colloids Surf., A* **2011**, *377*, 115−122.
(39) Liu, J.; Xu, Z.; Masliyah, J. *Langmuir* **2003**, *19*, 3911−3920.
(40) Liu, J.; Xu, Z.; Masliyah, J. *Colloids Surf., A* **2005**, *260*, 217−228.
(41) Hassenkam, T.; Andersson, M. P.; Hilner, E.; Matthiesen, J.; Dobberschütz, S.; Dalby, K. N.; Bovet, N.; Stipp, S. L. S.; Salino, P.; Reddick, C.; Collins, I. R. *SPE Journal* **2016**, *21* (03), 720−729.
(42) Pedersen, N. R.; Hassenkam, T.; Ceccato, M.; Dalby, K. N.; Mogensen, K.; Stipp, S. L. S. *Energy Fuels* **2016**, *30* (5), 3768−3775.
(43) Shi, L.; Olsson, M. H. M.; Hassenkam, T.; Stipp, S. L. S. *Energy Fuels* **2016**, *30*, 5346.
(44) Seiedi, O.; Rahbar, M.; Nabipour, M.; Emadi, M. A.; Ghatee, M. H.; Ayatollahi, S. *Energy Fuels* **2011**, *25*, 183−188.
(45) Kumar, K.; Dao, E.; Mohanty, K. K. *J. Colloid Interface Sci.* **2005**, *289*, 206−217.
(46) Lord, D. L.; Buckley, J. S. *Colloids Surf., A* **2002**, *206*, 531−546.
(47) Israelachvili, J. N. *Intermolecular and Surface Forces*, 2nd ed.; Academic Press: New York, 1992.
(48) Cappella, B.; Dietler, G. *Surf. Sci. Rep.* **1999**, *34*, 1−104.
(49) Hassenkam, T.; Pedersen, C. S.; Dalby, K.; Austad, T.; Stipp, S. L. S. *Colloids Surf., A* **2011**, *390*, 179−188.
(50) Hassenkam, T.; Mitchell, A. C.; Pedersen, C. S.; Skovbjerg, L. L.; Bovet, N.; Stipp, S. L. S. *Colloids Surf., A* **2012**, *403*, 79−86.
(51) Basu, S.; Sharma, M. M. *J. Colloid Interface Sci.* **1996**, *181*, 443−455.
(52) Basu, S.; Sharma, M. M. *SPE Journal* **1997**, *2*, 427−435.
(53) Basu, S.; Sharma, M. M. *SPE Journal* **1999**, *4* (3), 235−241.
(54) Hartley, P. G.; Grieser, F.; Mulvaney, P.; Stevens, G. W. *Langmuir* **1999**, *15*, 7282−7289.
(55) Hogshead, C. G.; Manias, E.; Williams, P.; Lupinsky, A.; Painter, P. *Energy Fuels* **2011**, *25*, 293−299.
(56) Liu, J.; Xu, Z.; Masliyah, J. *J. Colloid Interface Sci.* **2005**, *287*, 507−520.
(57) Liu, J.; Zhang, L.; Xu, Z.; Masliyah, J. *Langmuir* **2006**, *22*, 1485−1492.
(58) Long, J.; Xu, Z.; Masliyah, J. H. *Colloids Surf., A* **2006**, *281*, 202−214.
(59) Ta, T. C.; Sykes, M. T.; McDermott, M. T. *Langmuir* **1998**, *14*, 2435−2443.
(60) Liu, L.; Buckley, J. S. *J. Pet. Sci. Eng.* **1999**, *24*, 75−83.
(61) Dagastine, R. R.; Stevens, G. W.; Chan, D. Y. C.; Grieser, F. *J. Colloid Interface Sci.* **2004**, *273* (1), 339−342.
(62) Watson, G. S.; Watson, J. A. *Quantitative Measurements of Nano Forces using Atomic Force Microscopy (AFM)*; VDM Verlag: Saarbrücken, 2008.
(63) Ducker, W. A.; Senden, T. J.; Pashley, R. M. *Nature* **1991**, *353* (6341), 239−241.
(64) Adamson, A.; Gast, A. *Physical Chemistry of Surfaces*, 6th ed.; Wiley-Interscience: New York, 1997.
(65) Butt, H.-J.; Cappella, B.; Kappl, M. *Surf. Sci. Rep.* **2005**, *59*, 1−152.
(66) Sayyouh, M. H.; Hemeida, A. M.; Al-Blehed, M. S.; Desouky, S. M. *J. Pet. Sci. Eng.* **1991**, *6* (3), 225−233.
(67) Buckley, J. S.; Wang, J. *J. Pet. Sci. Eng.* **2002**, *33* (1−3), 195−202.
(68) Salathiel, R. A. *JPT, J. Pet. Technol.* **1973**, *25* (10), 1216−1224.
(69) Buckley, J. S.; Takamura, K.; Morrow, N. R. *SPE Reservoir Eng.* **1989**, *4* (03), 332−340.
(70) Buckley, J. S.; Lord, D. L. *J. Pet. Sci. Eng.* **2003**, *39*, 261−273.

DOI: 10.1021/acs.energyfuels.6b01862
Energy Fuels 2016, 30, 9193−9202